

The gravitational-wave spectrum of a non-axisymmetric torus around a rapidly spinning black hole

Omer Bromberg¹, Amir Levinson¹ and Maurice van Putten²

ABSTRACT

The gravitational-wave spectrum emitted by a non-axisymmetric torus rotating at an angular velocity Ω_T , is derived in terms of a structure function representing a combination of sausage-tilt modes in the torus in the limit of an incompressible fluid. The analysis of the gravitational-wave spectrum is then applied to a model proposed recently, in which a highly magnetized torus interacts with a stellar mass, Kerr black hole via poloidal field lines that connect the torus and the horizon. The deformation of the torus results from global magnetic instabilities when the magnetic field strength inside the torus exceeds a few times 10^{15} Gauss. The dynamics of the system is illustrated using a non-MHD toy model. It is found that, quite generally, most of the gravitational-wave energy emitted is in the frequency range of sensitivity of LIGO and Virgo.

Subject headings: black hole physics - gamma rays: bursts - gravitational waves

1. Introduction

Formation of systems consisting of a rapidly rotating, stellar mass black hole surrounded by a magnetized torus, is thought to be the outcome of catastrophic events like black hole-neutron star and neutron star-neutron star coalescence (e.g., Eichler et al. 1989; Paczyński 1991) or core collapse of massive stars (Woosley 1993). Such episodes are expected to be accompanied by bursts of intense emissions of photons, neutrinos and gravitational waves, of which GRBs may be an example. The free energy source that powers those systems may be the binding energy associated with the compact object or its rotational energy. The possibility that GRBs and microquasars are powered by the rotational energy of a Kerr black hole attracted much attention in recent years (e.g., Levinson & Eichler 1993; Levinson & Blandford 1996; Meszaros & Rees 1997; Van Putten 2000, 2001; Lee, et al. 2000; Brown,

¹School of Physics & Astronomy, Tel Aviv University, Tel Aviv 69978, Israel; Levinson@wise.tau.ac.il

²LIGO Laboratory, MIT 17-161, Cambridge, MA 02139, USA

et al. 2000; Lyutikov & Blandford 2003). The extraction of the hole rotational energy in those scenarios is accomplished through the Blandford-Znajek process (Blandford & Znajek, 1977), in which energy is transferred from the horizon outward along magnetic field lines that penetrate the horizon. While the total energy available depends solely on the angular momentum of the hole, the rate at which the energy can be extracted depends also on the strength of the magnetic field. In order to account for the characteristic GRB luminosities observed, the strength of the magnetic field inside the ergosphere should be on the order of 10^{15} G. That such strong magnetic fields can be produced in rapidly rotating, dense objects appears to be supported by recent observations of magnetars that indicate the presence of a dipole component with field strength in excess of 10^{15} G. How those fields are generated is yet an open issue.

The details of the interaction of the black hole and the magnetized torus depend in addition on the topology of the magnetic field (see e.g., Levinson 2005 for a recent account). Two inherently different disk magnetizations are discussed in the literature. The first one consists of what we term an open-field magnetosphere, in which there is no link between the horizon and the disk. In the second one, termed closed-field, a large portion of magnetic field lines that thread the horizon are anchored to the torus (Nitta et al. 1991; van Putten 1999, 2001; Uzdensky 2004). In the latter case, a considerable fraction of the extracted energy can be reprocessed by the surrounding torus, as explained below. The astrophysical consequences of the closed field model have been examined recently (Van Putten 2001; Van Putten & Levinson 2003). In particular, it has been shown that nonlinear deformations of the torus can lead to a prodigious gravitational wave emission. In this paper we consider the possibility that dynamical deformations result from magnetic instabilities, and calculate the gravitational wave spectrum emitted from the torus using a toy model.

2. High-Mass Tori in Suspended Accretion

A key feature of the suspended accretion model is a direct magnetic link between a relatively high mass torus (a few percent of the BH mass) and the horizon. In this state, the torus contains a net poloidal magnetic flux, supported by a uniform magnetization topologically equivalent to two counter-oriented current rings in the equatorial plane (van Putten & Levinson 2002, 2003). In general the vacuum magnetosphere consists of two separated regions of closed field lines; at large radii (compared with the radius of the outer current ring) the field quickly approaches a dipole solution. In the inner region the field lines intersect the horizon, giving rise to a strong coupling between the black hole and the inner face of the torus. The vacuum magnetosphere of the rotating torus is, however, unstable by virtue

of the strong parallel electric fields induced by the torus rotation, and the hot torus corona. The resultant plasma ejection will lead to opening of some field lines, thereby altering the magnetospheric structure, as described in great detail in (van Putten & Levinson 2003). In particular, a cylindrical current sheet is expected to form in the polar region, supporting an open flux tube that extends from the horizon to infinity (see also Uzdensky 2004). Now, the magnetic field inside the torus cannot be purely poloidal, because purely poloidal fields are unstable and tend to decay completely in a few Alfvén timescales (Markey & Tayler, 1973; Flowers & Ruderman, 1975; Eichler 1982). However, by conservation of helicity, a twisted magnetic field does not decay to zero, at least in the limit of ideal magnetohydrodynamics. Instead, it will evolve into a new, stable configuration. Recent 3D MHD simulations (Braithwaite & Spruit, 2004) show that magnetic fields inside stars tend to develop a belt of twisted field lines that stabilize a dipolar field in the magnetosphere above the stellar surface. This configuration appears to be stable over the resistive timescale, which is typically much longer than the canonical dynamical timescales (e.g., rotation periods and acoustic timescales). By topological equivalence in poloidal cross-section, it is therefore conceivable that the magnetic field inside the torus is twisted as well, supporting an overall torus magnetosphere which, from the outside, is consistent with a uniformly magnetized surface of the torus.

In cases where the black hole rotates faster than the torus, as anticipated for the systems under consideration, energy and angular momentum are transferred from the hole into the inner face of the torus, tending to spin it up. In the suspended accretion model (van Putten & Ostriker 2001), the energy deposited in the torus is emitted predominantly in the form of gravitational waves, owing to large deformations of the torus, as well as MeV neutrinos and baryon rich winds to infinity, resulting from the rapid heating of the torus by the friction between its layers (van Putten & Levinson 2003). The luminosity and spectrum of the gravitational waves depend on the multipole mass moments in the torus (the gravitational wave luminosity cannot exceed of course the power supplied by the black hole). Finite number of multipole mass moments can be generated by the Papaloizou-Pringle instability (Papaloizou & Pringle 1984) under certain conditions (van Putten 2002). Here we consider torus deformations resulting from global magnetic instabilities, that sets in when the magnetic field exceeds a certain value.

When the magnetic field inside the torus exceeds 10^{15} G roughly, it becomes dynamically important. MHD instabilities would then tend to quickly destroy the field. Here, we speculate that the input from the black hole gives rise to some dynamo mechanism that sustains the field for times much longer than the orbital time. It is not clear at present whether such a dynamo process, even if exists, is stable in the sense that any destruction of the link between the hole and the torus may lead to a complete shut off of this induced dynamo process. Assuming that the field is sustained for many orbital times, it is likely

that magnetic stresses that builds up inside the torus will lead to nonlinear, dynamical deformations of the torus. The power spectrum of the induced mass moments is likely to be dominated by the several lowest multipoles. A naive estimate of the field strength above which the torus becomes unstable to deformations may be obtained by equating the torque acting on a perturb current ring, owing to the mutual magnetic interaction between the two current rings, with the gravitational torque exerted by the central black hole (van Putten & Levinson 2003). The presence of toroidal field components inside the torus may somewhat alter this estimate. Interestingly, this critical magnetic field corresponds to a spin down time of the order of tens of seconds for a stellar mass black hole, consistent with durations of long GRBs. Full 3D GRMHD simulations are ultimately needed to study the evolution of the system under consideration. To get some insight into the dynamical deformations of the torus in the nonlinear regime, we employed a toy model in which the inner and outer faces of the torus are represented as two fluid rings, each carrying electric current with equal magnitude but opposite orientation. Although this numerical model has probably very little relevancy for any realistic situation, it provides a framework for simple calculations. The simulations described below reveal the existence of a nonlinear, oscillatory phase that sets in when the magnetic field approaches the critical value, as described below.

3. GW luminosity from the torus mass-moments

In this section we consider the gravitational wave spectrum emitted by a rotating, non-axisymmetric torus. We derive a general result for the multipole emission, that we express in terms of the relevant scales involved and a structure function that depends on the detailed configuration of the torus. We then calculate analytically the structure function using a simple, illustrative torus configuration. In the next section we shall use this result together with our simple dynamical model to obtain an order of magnitude estimate for the multipole gravitational wave emission associated with the deformations caused by the global magnetic instability discussed above.

In the non-relativistic limit, the mass-moment of order l, m associated with the mass distribution of the deformed torus can be expressed as,

$$I_{lm} = \frac{16\pi}{(2l+1)!!} \left[\frac{(l+1)(l+2)}{2(l-1)l} \right]^{1/2} \int \rho Y_{lm}^* r^l d^3x, \quad (1)$$

where $\rho = \rho(t, \mathbf{r})$ is the density of the torus, measured in the black hole frame. The corresponding gravitational wave power is given by (Thorne 1980)

$$\frac{dE_{lm}}{dt} = \frac{1}{32\pi} \frac{G}{c^{2l+1}} \left(\frac{d^{l+1}}{dt^{l+1}} I_{lm} \right)^2 ; l \geq 2. \quad (2)$$

To simplify the analysis we make the following assumptions: First, we suppose that the rotational period of the torus is considerably shorter than characteristic evolution time of the system, so that the evolution of the torus can be considered adiabatic. This means that over time intervals shorter than the evolution time, the gravitational wave emission can be computed assuming a fixed torus configuration. We can then ignore, to a good approximation, the intrinsic time change of the various mass moments. Under this approximation, each time derivative of I_{lm} in eq. (2) brings an additional power of $\Omega_m \equiv m\Omega_T$, where Ω_T denotes the average angular velocity of the torus (e.g., Thorne 1980). Over longer timescales the spectrum of the gravitational waves also evolves adiabatically, owing to the temporal changes of the torus configuration. Second, we assume that at any given time the density inside the torus is uniform. This may be justified if (i) the heating of the torus resulting from the dissipation of the energy extracted from the central black hole is uniform, and (ii) the sound crossing time is short compared with the evolution time, so that any local changes in pressure produced by deformations of the torus adjust instantaneously. Of course, the density must evolve also in time to keep the total mass of the torus fixed (we ignore any mass loss or accretion).

In the following we consider emission from a non-evolving torus (i.e., fixed configuration), rotating at a frequency Ω_T . The total luminosity in a gravitational wave mode of frequency $\Omega_m = m\Omega_T$ is,

$$L_m = \sum_{l=m}^{\infty} \frac{dE_{lm}}{dt} = \frac{G}{32\pi} \sum_{l=m}^{\infty} \left(\frac{m\Omega_T}{c} \right)^{2l+2} cI_{lm}^2. \quad (3)$$

We find that most of the contribution to L_m comes from the first term ($l = m$). It is therefore sufficient to compute only I_{mm} . Under the above assumptions eq. (1) for the $l = m$ component reduces to,

$$I_{mm} = C_{mm}\rho \int_0^{2\pi} e^{-im\phi} d\phi \int_{\theta_{min}(\phi)}^{\theta_{max}(\phi)} (\sin\theta)^{m+1} d\theta \int_{r_1(\theta,\phi)}^{r_2(\theta,\phi)} r^{m+2} dr, \quad (4)$$

where C_{mm} is a normalization constant:

$$C_{mm}^2 = 32\pi \frac{(m+1)(m+2)}{m(m-1)(2m+1)(2m)!}. \quad (5)$$

The limits of integration are shown schematically in fig. 1 for a torus with a circular cross section. For the situations envisaged here, we typically have $r_2 - r_1 \ll r_2 + r_1$. It is convenient therefore to use the variables

$$b(\theta, \phi) = (r_2 + r_1)/2; \quad d(\theta, \phi) = (r_2 - r_1)/2. \quad (6)$$

For $d/b \ll 1$ the integration over dr in eq. (4) can be expanded in powers of d/b . To first order we obtain,

$$I_{mm} = 2C_{mm}\rho \int_0^{2\pi} F_m(\phi)e^{-im\phi}d\phi, \quad (7)$$

with the structure function given by

$$F_m(\phi) = \int_{\theta_{min}(\phi)}^{\theta_{max}(\phi)} (\sin \theta)^{m+1} b(\theta, \phi)^{m+2} d(\theta, \phi) d\theta. \quad (8)$$

As an illustrative example for which the structure function can be calculated analytically, we consider a torus having a circular cross section of radius a . The cross-sectional radius is allowed to depend on the azimuthal angle, viz., $a = a(\phi)$. In addition, we allow for the center of the circle to be locally shifted above the equatorial plane of the black hole at an angle $\psi_c(\phi)$, but assume its distance from the rotational axis of the hole, denoted by R_T , to be independent of ϕ (see fig 1). For this configuration we then find,

$$b(\theta, \phi) = R_T \frac{\sin(\theta + \psi_c)}{\cos(\psi_c)}, \quad (9)$$

$$d(\theta, \phi) = a \sqrt{1 - \frac{1}{\epsilon^2} \cos^2(\theta + \psi_c)}, \quad (10)$$

where $\epsilon = (a/R_T) \cos(\psi_c) \ll 1$. Substituting the latter results into eq. (8) yields

$$F_m(\phi) = R_T^{m+1} (1 + \tan^2 \psi_c)^{\frac{m+1}{2}} a^2 \int_{\psi_c - \pi/2}^{\psi_c + \pi/2} (1 - \epsilon^2 \sin^2 \chi)^{m+1} \cos^2 \chi d\chi. \quad (11)$$

Using $\epsilon^2 \ll 1$ and $\tan^2 \psi_c \ll 1$ as small parameters, and keeping only first order terms we finally arrive at,

$$F_m(\phi) = \frac{\pi R_T^{m+1}}{2} a^2 \left(1 + \frac{m+1}{2} \tan^2 \psi_c \right). \quad (12)$$

As seen the structure function depends to leading order only on the two functions $a^2(\phi)$ and $\tan^2 \psi_c$. These functions are periodic in ϕ and can be expressed in terms of their Fourier expansions as,

$$a^2(\phi) = \sum_n a_n^2 e^{in\phi}; \quad \tan^2 \psi_c(\phi) = \sum_k \delta_k^2 e^{ik\phi}. \quad (13)$$

To zeroth order in $\tan^2 \psi_c$, the total mass of the torus is given by, $M_T = 2\pi^2 R_T \rho a_0^2$, where a_0 is the Fourier coefficient of the $n = 0$ term above. Using eqs. (7), (8), (12) and (13), we can express the mass moments in terms of R_T and M_T as:

$$I_{mm} = C_{mm} M_T R_T^m \left[\frac{a_m^2}{a_0^2} + \frac{m+1}{2} \sum_{k=0}^m \frac{a_k^2}{a_0^2} \delta_{m-k}^2 \right] \equiv C_{mm} M_T R_T^m \zeta_m. \quad (14)$$

Substituting the latter equation into eq. (15), yields the gravitational wave luminosity of the order m multipole:

$$L_m = \frac{GM_T^2 \Omega_T (m+1)(m+2)m^{2m+1}}{R_T (m-1)(2m+1)(2m)!} \left(\frac{v_T}{c}\right)^{2m+1} \zeta_m^2, \quad (15)$$

where $v_T = R_T \Omega_T$ is the Keplerian velocity. It can be seen that for $v_T/c < 0.7$ the quantity L_m/ζ_m^2 decreases rapidly with increasing m . We anticipate, therefore, that for any realistic deformation, the gravitational wave spectrum will be dominated by the quadrupole moment. For our canonical choice of parameters, the quadrupole luminosity of the torus is

$$L_2 = 5 \times 10^{52} \left(\frac{M_H}{7M_\odot}\right)^3 \left(\frac{M_T}{0.03M_H}\right)^2 \left(\frac{\eta}{0.1}\right)^{10/3} \zeta_2^2 \text{ erg s}^{-1}, \quad (16)$$

where $\eta = \Omega_T/\Omega_H$ is the ratio of torus and black hole angular velocities. If the deformation caused by magnetic instabilities is dominated by the lowest few mass moments, then $\zeta_2 \sim 0.1$ is anticipated. In what follows we employ our toy model to calculate dynamic deformations of the torus, and the resultant gravitational wave spectrum.

4. Nonlinear Evolution of Magnetic Tilt Modes

4.1. Numerical Simulations and Results

In our numerical model, the inner and outer faces of the torus are represented as two rotating fluid rings, each carrying electric current of the same magnitude but opposite orientation. The rings have the same density, with a total mass (the sum of the two rings) M_T . The two rings are allowed to rotate with different angular velocities, representing the differential rotation of the torus in its suspended accretion state (van Putten & Ostriker 2001). The difference in angular velocities of the undisturbed torus is expected to be on the order of $\Delta\Omega \sim \Omega_T \delta$, where Ω_T is the average angular velocity and $\delta \ll 1$ a slenderness ratio, equals roughly the ratio of the characteristic dimension of the torus cross section and its outer radius R_T in the initial state. The angular velocity of the outer (+)/inner (-) ring is then given by $\Omega_\pm = \Omega_T \mp \Delta\Omega/2$. Each ring is divided into N identical segments (see fig. 2) that rotate with the corresponding angular velocity around the symmetry axis of the system, and in addition are free to move in the vertical direction. Every segment in a given ring is subject to the gravitational force exerted by the black hole and the magnetic force contributed by all segments in the other ring. To avoid technical difficulties we ignored self interactions that, like the self inductance, diverge as the cross-sectional radius of the ring shrinks to zero. We further use the initial value of the magnetic field in the center between

the rings, at $r = R_T$, as a measure for the average magnetic field in the torus in its initial state, thereby avoiding the need to deal with renormalization of the ring parameters. Our model does not account for the input from the BH and losses to infinity in a self consistent manner. We suppose that in the suspended accretion state, the horizontal component of the net force acting on each ring is balanced by centrifugal forces which are not accounted for in our model. Under this assumption, the rings segments are restricted to move only horizontally (in the z direction) in addition to their rotation; that is, each segment is maintained at a fixed cylindrical radius throughout its motion. The details of our numerical model are described in the appendix.

The dynamics of the system has been studied for a range of magnetic fields and δ , and our canonical choice of the remaining parameters. Below we present results for the case $\Delta\Omega = 0$, although we have examined also cases with differential rotation. Quite generally, we find that differential rotation leads to a somewhat faster disruption of the rings, but whether this has any significance in a more realistic situations is not clear. At any rate, full 3D MHD simulations with a more realistic magnetic field configuration inside the torus are ultimately required for a complete treatment of the torus dynamics. Our purpose here is merely to illustrate some very general properties relevant to the gravitational wave emission.

The rings segments are taken to lie initially in the equatorial plane ($z = 0$), and a small perturbation $\Delta z_i \ll z_i$ is then applied to the i th segment. Analytic solutions obtained for small magnetic fields have been reproduced numerically as a check on our code. As expected, for magnetic fields well below the critical value the oscillation of the rings segments are linear with a Keplerian frequency. For magnetic fields well above the critical value, the rings disrupts over a few orbital periods. We find, however, a range of magnetic fields around the critical value for which the system exhibits a nonlinear, oscillatory phase lasting for hundreds to thousands orbital periods, depending on the choice of parameters. The amplitude of these oscillations is larger by many orders of magnitudes than the initial perturbation. An example of a nonlinear deformation seen at some particular time in a typical run is depicted in fig 2.

The gravitational wave spectrum emitted by the torus during the nonlinear oscillatory phase is computed as follows: we divide time into many short time intervals of equal duration Δt , where typically Δt is on the order of several orbital periods. Within each time interval the torus configuration is taken to be fixed. We have made several checks and verified that the resultant gravitational wave spectrum converges as we increase the number of time intervals (decrease Δt). The average gravitational wave luminosity, $L_m(\Delta t_i)$, emitted over a given time interval Δt_i , is then calculated using eqs. (13)-(15), where $a(\phi)$ in eq. (13) is taken to be half the distance between segments of the inner and outer rings located at a given ϕ (see fig. 1), and $\psi_c(\phi)$ is the shift of the central point above the equatorial plane. We

then let the system evolve until a new configuration is obtained at Δt_{i+1} , and calculate the gravitational wave luminosity emitted over the new time interval. The process is repeated until the system disrupts or until the spin down time is exceeded, whichever comes first. The total energy associated with the order m mass moment is given by

$$E_m = \sum_i L_m(\Delta t_i) \Delta t_i. \quad (17)$$

Figure 3 shows the temporal evolution of ζ_m^2 for rigid rotation, $\Delta\Omega = 0$, and different values of the slenderness ratio δ . Each panel shows the power spectrum averaged over the time intervals indicated. The transition to the non-linear phase is clearly seen. The corresponding gravitational wave spectra, integrated over the entire duration of the nonlinear oscillations, are exhibited in figure 4. The total duration of the event is indicated for each case. The quantity plotted is E_m/E_0 versus m , where E_m is given by eq. (17), and the scaling factor by,

$$E_0 = \frac{GM_T^2 \Omega_T}{R_T} T = 2.4 \times 10^{54} \left(\frac{M_T}{0.03 M_H} \right)^2 \left(\frac{\eta}{0.1} \right)^{5/3} T \quad \text{ergs.} \quad (18)$$

with T being the overall duration of the burst measured in seconds. As seen in the figure, the gravitational wave spectrum is dominated by the quadrupole mass moment. For the cases shown, the total energy emitted over the spin down time of the hole is of the order of $10^{52.5}$ ergs.

4.2. Application to the suspended accretion model

Quite generally, core-collapse of a massive star is believed to produce a black hole, parametrized by its mass M , specific angular momentum a and kick velocity K . The latter is due to the Bekenstein gravitational-radiation reaction force, and assumes typical values of a few hundred km/s (Bekenstein 1973). Thus, the best theoretical candidate for an active stellar nucleus is a newly formed rapidly spinning high-mass black hole with low kick velocity (van Putten 2004). By numerical integration, these can be seen to form with rotational energies

$$E_{rot} = 2M \sin^2(\lambda/4), \quad \sin \lambda = a/M, \quad (19)$$

of about $\epsilon_{rot} \sim 0.33 - 0.67$ times the rotational energy of an extreme Kerr black hole in compact binaries with periods of about 1d or less. If so, the small branching ratio of Type Ib/c supernovae into GRB-supernovae can be identified with the sub-sample of black holes having small kick velocities.

The suspended accretion state represents an equilibrium between incoming flux in energy and angular momentum, and outgoing flux in various emission channels. As such, the luminosity in gravitational radiation, representing the dominant output of these emissions due the relativistic compactness of the torus, is set uniquely according to the scaling relation (van Putten, et al. 2004)

$$E_{gw} = 4 \times 10^{53} \left(\frac{M_H}{7M_\odot} \right) \left(\frac{\eta}{0.1} \right) \epsilon_{rot}, \quad (20)$$

where the canonical values of $M_H = 7M_\odot$ and $\epsilon_{rot} \simeq 0.5$ are supported by numerical integrations of the conservation laws of mass and angular momentum in core-collapse supernovae (van Puttem 2004). We recall that the lifetime of rapid spin of the black hole surrounded by a torus operating at about the critical poloidal magnetic field-energy satisfies (van Putten & Levinson 2003)

$$T_s = 90\text{s} \epsilon_{rot} \left(\frac{M_H}{7M_\odot} \right) \left(\frac{\eta}{0.1} \right)^{-8/3} \left(\frac{M_T}{0.03M_H} \right)^{-1}. \quad (21)$$

Upon identifying the duration of the burst with T_s , substituting the latter into eq. (18), and defining the dimensionless energy $\kappa_2 = E_{gw}/E_0$, we have the following reduction:

$$\left(\frac{\kappa_2}{10^{-3}} \right) \left(\frac{M_T}{0.03M_H} \right) = \left(\frac{\eta}{0.1} \right)^2. \quad (22)$$

Our present numerical results are contained in the factor $\kappa_2 = E_{gw}/E_0 \simeq E_2/E_0 \sim 10^{-4}(\eta/0.1)^{5/3}$. The results (22) are consistent with a torus mass on the order of a few percent of the black hole mass and efficiency factors on the order of a few percent. Formally, our model is hereby left with one free parameter, e.g., M_T , or η . A further reduction in parameters requires more advanced numerical simulations.

5. conclusion

In this work, we examined the gravitational-wave spectrum of a torus surrounding a rapidly rotating black hole, thought to form in core-collapse supernovae. We focused on high-mass black holes with high rotation rates and low kick velocities, so that a black hole plus torus system can be reasonably expected to form. We further assumed the presence of a dynamo mechanism, otherwise unknown, to consider the possibility of superstrong, ordered magnetic fields in sufficiently massive tori. Under these rare circumstances, in light of the observed small branching ratio of GRB-supernovae from their parent population of Type Ib/c supernovae, we considered the suspended accretion model in which the duration

of the burst is identified with the lifetime of rapid spin of the black hole (van Putten & Levinson, 2003). In this model, the black hole-spin energy is catalytically converted into various emission channels by the torus, and notably so into gravitational radiation, through a direct magnetic link between the torus and the event horizon.

Quite generally, we find that for sufficiently strong magnetic fields, the torus develops spontaneously non-axisymmetric tilt instabilities due to magnetic moment-magnetic moment self-interactions. These distortions may eventually disrupt and destroy the torus on time scales longer than the orbital period and shorter than the lifetime of rapid spin of the black hole. This might account for the observed intermittent behavior seen in GRB lightcurves.

During the numerically observed non-linear oscillatory phase, the torus radiates intense gravitational radiation, provided its mass has accumulated to a few percent of the mass of the central black hole. Our calculations are based on a non-MHD, double-ring model representing a uniformly magnetized torus in suspended accretion. The numerical simulations display a spectrum of multipole mass-moments, from which we were able to calculate the gravitational-wave spectrum following a somewhat more general analytic expression for the gravitational-wave emissions as a function of both sausage and tilt modes.

We generally find that the nonlinear phase during which gravitational-wave emission ensues, lasts for many orbital times, but may be shorter than the spin down time of the hole, though not by a very large factor. In particular, differential rotation increase the tendency of the rings to disperse, thus decreasing the magnetic field-energy and the total gravitational-wave energy produced in the burst. Whether this tendency remains in a more realistic situation is unclear, given the simplicity of our model. It is anyhow conceivable that if the torus disrupts after time shorter than the black hole spin down time, it may be rebuilt due to continuing infall in the core-collapse event, an effective dynamo may again rebuild a superstrong magnetic field, up to the critical value in a few tenths of seconds (van Putten & Levinson, 2003). If so, the energy extraction process and gravitational-wave emissions can reoccur. Such sequential bursts may continue as long as there is enough rotational energy in the black hole (and as long as there is continuing infall of matter to regenerate the torus).

The energy flux of the radiated energy is determined by the mass-moment times the velocity factor $(v_T/c)^{2m+1}$. Since $v_T \simeq 0.4c$, terms with high azimuthal quantum number m make virtually no contributions to the radiated energy, and the gravitational-wave spectrum will be dominated by the lowest mass-moments. In particular, a dominant fraction should be emitted by the $m = 2$ term with frequency of about 650Hz for our canonical choice of parameters. This prediction happens to be around the minimum of the strain-amplitude noise of the broad band detectors LIGO and Virgo (Abramovici, et al. 1992; Barish & Weiss 1999; Bradaschia et al., 2002; Acernese et al., 2002), as well as GEO (Danzmann,

1995; Willke et al. 2002) and TAMA (Ando et al., 2002). For typical parameters of stellar mass black holes, consistent with numerical estimates in the core-collapse scenario of GRB-supernovae, the gravitational-wave emissions are predicted to be detectable by advanced LIGO/Virgo detectors out to distances of about 100Mpc, corresponding to about 1 event per year (van Putten et al. 2004).

We can summarize our numerical results in terms of the single fraction $\kappa_2 = E_2/E_0$, representing the energy emitted in quadrupole gravitational-wave emission relative to the scale factor E_0 . The numerical results indicate values on the order of $\kappa_2 \sim 10^{-4}(\eta/0.1)^{5/3}$. These values are consistent with a torus mass reaching a few percent of the mass of the central black hole, and efficiencies in converting spin energy into gravitational radiation of about a few percent.

This research was supported by an Israel Science Foundation Center of Excellence Award.

A. The double-ring model

Here we formulate the equation of motions of the rings: The inner (outer) ring is considered to be composed of $N_1(N_2)$ linear segments, with equal mass and, initially, equal length. (as seen in Fig. 5). We introduce two sets of indexes. Lower indexes, marked as i, j , stand for the ring's number (1,2). High indexes, marked as m, n , identify the number of each parameter within a specific ring. They run from 1 to $N_1(N_2)$ for the inner(outer) ring. Each ring is identified by N_i point elements, located on the joints between its segments. Their coordinates are denoted by: $\mathbf{r}_i^1 \dots \mathbf{r}_i^{N_i}$ and defined as:

$$\mathbf{r}_i^m = R_i \cos \phi_i^m \hat{\mathbf{x}} + R_i \sin \phi_i^m \hat{\mathbf{y}} + z_i^m \hat{\mathbf{z}}, \quad (\text{A1})$$

where ϕ is the azimuthal angle measured from the x axis (see fig.5 for illustration). Each segment is identified by the position of its center point:

$$\mathbf{S}_i^m = \frac{1}{2}(\mathbf{r}_i^{m+1} + \mathbf{r}_i^m); \quad m \in \{1 \dots N_i\}, \quad i \in \{1, 2\}, \quad (\text{A2})$$

while the segment length-vector is defined as:

$$\mathbf{L}_i^m = (\mathbf{r}_i^{m+1} - \mathbf{r}_i^m). \quad (\text{A3})$$

We also define a distance vector between two segments from different rings as:

$$\Delta \mathbf{S}_{ij}^{mn} = \mathbf{S}_i^m - \mathbf{S}_j^n. \quad (\text{A4})$$

Figure 5 shows an example for each of the vectors defined above. Initially, each segment has a size of $|\mathbf{L}_i^m| = \frac{2\pi R_i}{N_i}$, and since we consider the rings to be of equal mass density, all segments of the i 'th ring have a mass $m_i = \frac{M_T R_i}{(R_1 + R_2) N_i}$.

The motion of each ring is set by the motion of its N_i point elements. The gravitational acceleration of each point element due to the tidal forces exerted by the BH is:

$$(\ddot{z})_{i (grav)}^m = -\frac{GM_H}{|\mathbf{r}_i^m|^2} \frac{z_i^m}{|\mathbf{r}_i^m|} = -\frac{GM_H}{[R_i^2 + (z_i^m)^2]^{3/2}} \cdot z_i^m, \quad (\text{A5})$$

where R_i is the cylindrical radius of the i 'th ring.

The magnetic force acts between the current elements and not between point elements. Therefore, we first calculate the magnetic force induced on the segments of the rings (\mathbf{S}_i^m). The acceleration of each point element is simply the average acceleration of its adjoint segments. The magnetic force induced on segment \mathbf{S}_i^m in the i 'th ring by segment \mathbf{S}_j^n in the j 'th ring is:

$$\mathbf{F}_{ij}^{mn} = \frac{-I^2 \mathbf{L}_i^m \times (\mathbf{L}_j^n \times \Delta \mathbf{S}_{ij}^{mn})}{c^2 |\Delta \mathbf{S}_{ij}^{mn}|^3} = \frac{I^2 (\mathbf{L}_i^m \cdot \Delta \mathbf{S}_{ij}^{mn}) \mathbf{L}_j^n - (\mathbf{L}_i^m \cdot \mathbf{L}_j^n) \Delta \mathbf{S}_{ij}^{mn}}{c^2 |\Delta \mathbf{S}_{ij}^{mn}|^3}. \quad (\text{A6})$$

Each segment is influenced by the forces from all other segments in the second ring, therefore the total acceleration along the z axis of segment \mathbf{S}_i^m is:

$$(\ddot{S}_z)_{i (mag)}^m = \sum_{n=1}^{N_1} \mathbf{F}_{ij}^{mn} \cdot \hat{\mathbf{z}} = \frac{-I^2}{m_i c^2} \sum_{n=1}^{N_1} \left[\frac{(\mathbf{L}_i^m \cdot \Delta \mathbf{S}_{ij}^{mn}) (L_z)_j^n - (\mathbf{L}_i^m \cdot \mathbf{L}_j^n) (\Delta S_z)_{ij}^{mn}}{|\Delta \mathbf{S}_{ij}^{mn}|^3} \right], \quad (\text{A7})$$

where $i \neq j$, and we used the notation P_z to represent the z component of the vector \mathbf{P} . Therefore the acceleration of the point element with coordinate \mathbf{r}_i^m is:

$$\ddot{z}_{i (mag)}^m = \frac{1}{2} \left((\ddot{S}_z)_{i (mag)}^m + (\ddot{S}_z)_{i (mag)}^{m-1} \right), \quad (\text{A8})$$

where \mathbf{S}_i^m and \mathbf{S}_i^{m-1} are the two segments that have a common joint at \mathbf{r}_i^m (see fig.5 for clarification).

REFERENCES

- Abramovici, A., Althouse, W.E., Drever, R.W.P., et al., 1992, Science, 292, 325
 Acernese, F., et al., 2002, Class. Quant. Grav., 19, 1421
 Ando, M., and the TAMA Collaboration, 2002, Class. Quant. Grav., 19, 1409

- Antonelli, L.A., Piro, L., Vietri, M., et al., 2000, *ApJ*, 545, L39
- Barish, B., & Weiss, R., 1999, *Phys. Today*, 52, 44
- Bekenstein, J.D., 1973, *ApJ*, 183, 657
- Blandford, R. D., and Znajek, R. L. 1977, *MNRAS*, 179, 433
- Bradaschia, C., Del Fabbro, R., di Virgilio, A., et al., 1992, *Phys. Lett. A*, 163, 15
- Braithwaite, J., & Spruit, H.C. 2004, *Nature*, 431, 819
- Brown, G.E., Lee, C.-H., Wijers R.A.M.J., Lee, H.K., Israelian G. Bethe, H.A. 2000, *New Astron.*, 5, 191-210
- Danzmann, K., 1995, in *First Edoardo Amaldi Conf. Grav. Wave Experiments*, E. Coccia, G. Pizella, F. Ronga (Eds.), World Scientific, Singapore, p100
- Eichler, D., 1982, *ApJ*, 254, 683
- Eichler, D., Livio, M., Piran, T., Schramm, D. 1989, *Nature*, 340, 126
- Filipenko, A.V., 1997, *ARA&A*, 35, 309
- Flowers, E., & Ruderman, M., 1977, *ApJ*, 215, 302
- Lee, C.-H., Brown, G.E., & Wijers, R.A.M.J., 2002, *ApJ*, 575, 996
- Levinson, A., & Blandford, R. 1996, *ApJ*, 456, L29
- Levinson, A., & Eichler, D. 1993, *ApJ*, 418, 386
- Levinson, A., 2005, in ‘*Black Holes: Research and Development*, Nova Science Publishers, in press
- Markey, P. & Tyler, R.J., 1973, *MNRAS*, 163, 77
- Meszaros, P. & Rees M.J. 1997, *ApJ*, 476, 232
- Nitta, S-Y.; Takahashi, M.; Tomimatsu A. *Phys. Rev. D*. 1991, 44 2295-2305
- Papaloizou, J.C.B., & Pringle, J.E., 1984, *MNRAS*, 208, 721
- Paczyński, B.P., 1991, *Acta Astron.*, 41, 257-267
- Thorne, K.S., 1980, *RvMP*, 52, 299

- Uzdensky, D. A. 2004, *ApJ*, 620, 889
- van Putten, M.H.P.M., 1999, *Science*, 284, 115
- van Putten, M.H.P.M., & Ostriker, E.C., 2001, *ApJ*, 552, L31
- van Putten, M.H.P.M., 2001, *Phys. Rep.*, 345, 1; *ibid.* *Phys. Rev. Lett.*, 87, 091101
- van Putten, M.H.P.M., 2002, *ApJ*, 575, L71
- van Putten, M.H.P.M., & Levinson, A., 2002, *Science*, 295, 1874
- van Putten, M.H.P.M., & Levinson, A., 2003, *ApJ*, 584, 953
- van Putten, M.H.P.M., 2004, *ApJ*, 611, L81
- van Putten, M.H.P.M., Levinson, A., Lee, H.-K., Regimbau, T., & Harry, G., 2004, *Phys. Rev. D.*, 69, 044007
- Willke, B., et al., 2002, *Class. Quant. Grav.*, 19, 1377
- Woosley, S.E., 1993, *ApJ*, 405, 273

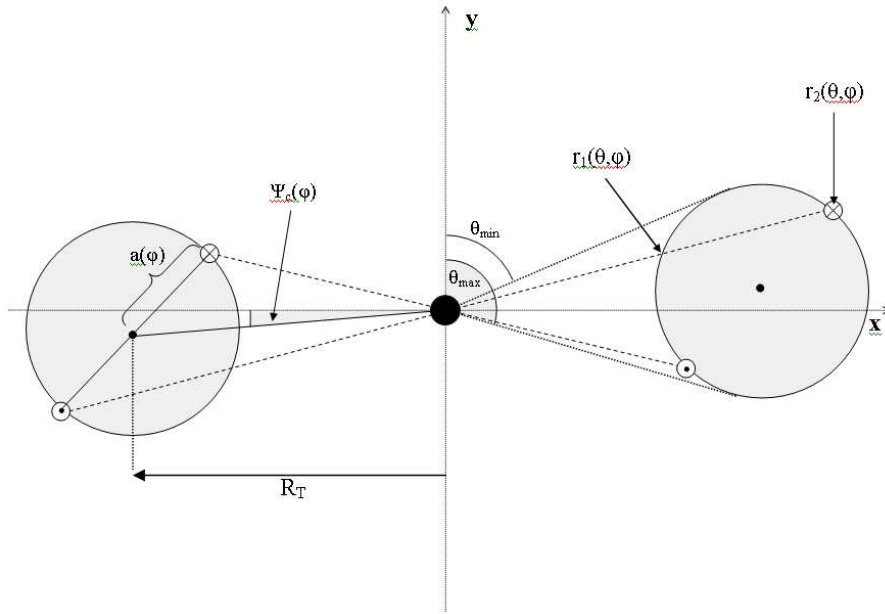


Fig. 1.— A cross sectional view of a system consisting of a black hole surrounded by a torus having a circular cross section. The coordinates used for the calculation of the gravitational wave emission are indicated (see text for further details). Also shown is the double ring system used in our dynamical model. The inner and outer rings are taken to lie on the surface of the torus, as indicated.

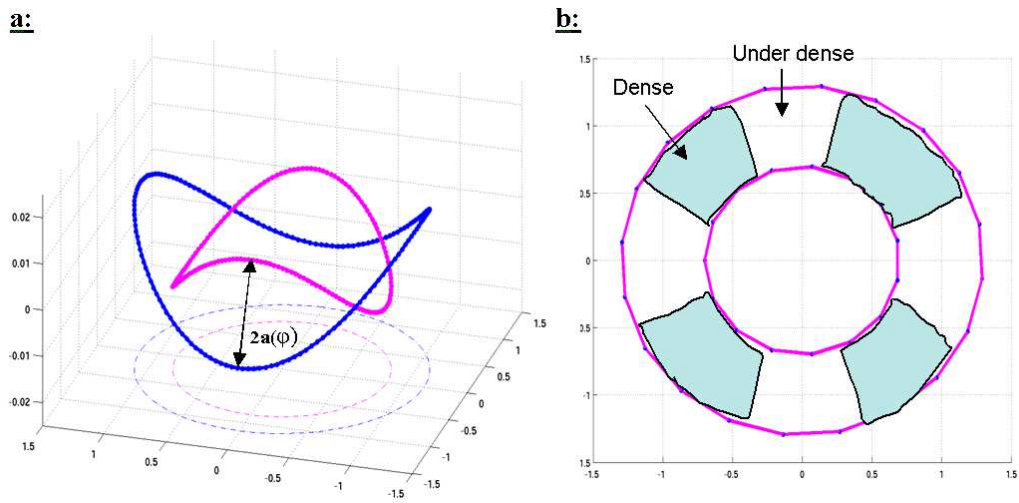


Fig. 2.— A typical ring configuration seen at some given time during the nonlinear oscillations.

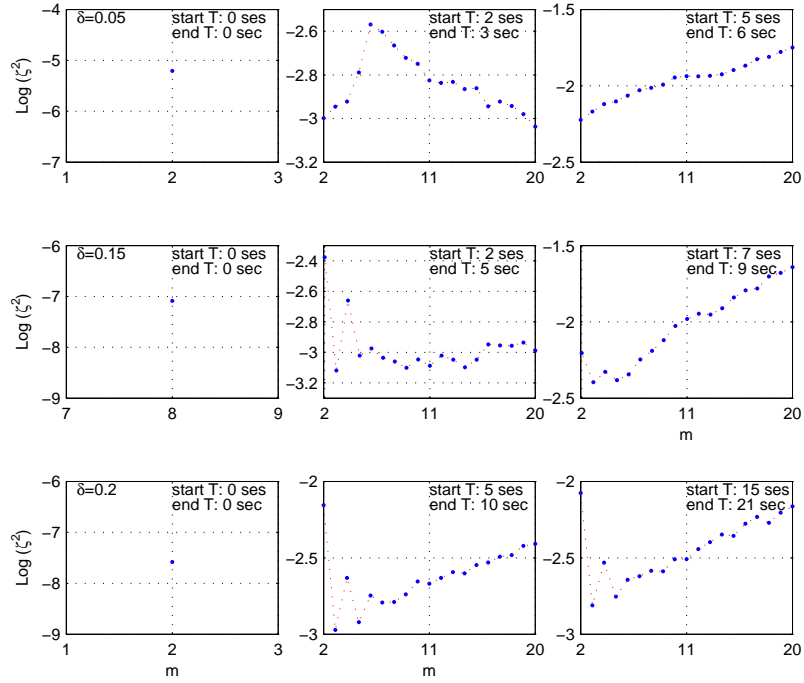


Fig. 3.— Plots of ζ_m^2 vs. azimuthal mode number m at different times, for $\delta = 0.05$ (upper set of panels), $\delta = 0.15$ (middle set of panels) and $\delta = 0.2$ (lower set of panels). Each panel shows the power spectrum averaged over the time intervals indicated. Left most panel in each set shows the initial state. Note that difference in initial perturbation in the two cases.

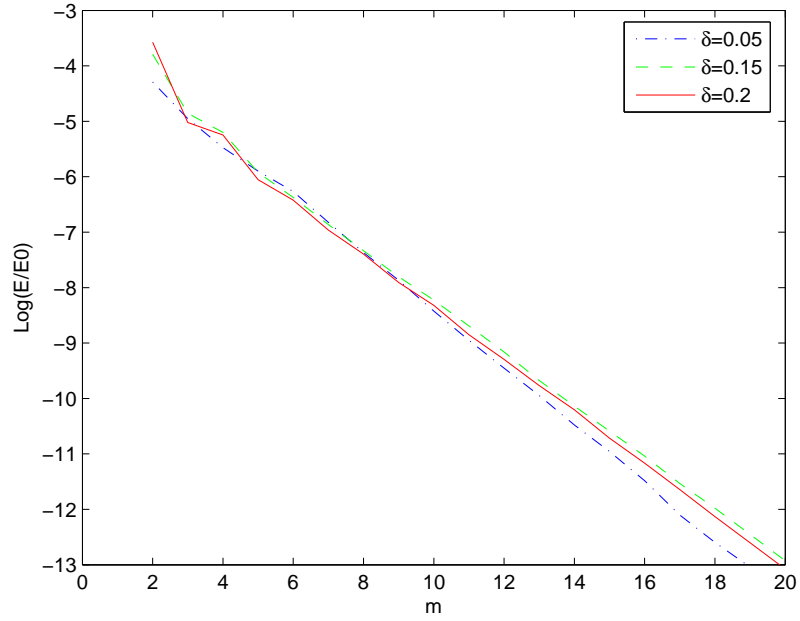


Fig. 4.— Energy spectra of gravitational waves, corresponding to the three cases exhibited in fig. 3. The gravitational wave energy is normalized by the scaling factor E_0 , given in eq. (18). As seen, the total power is dominated by the lowest moments.

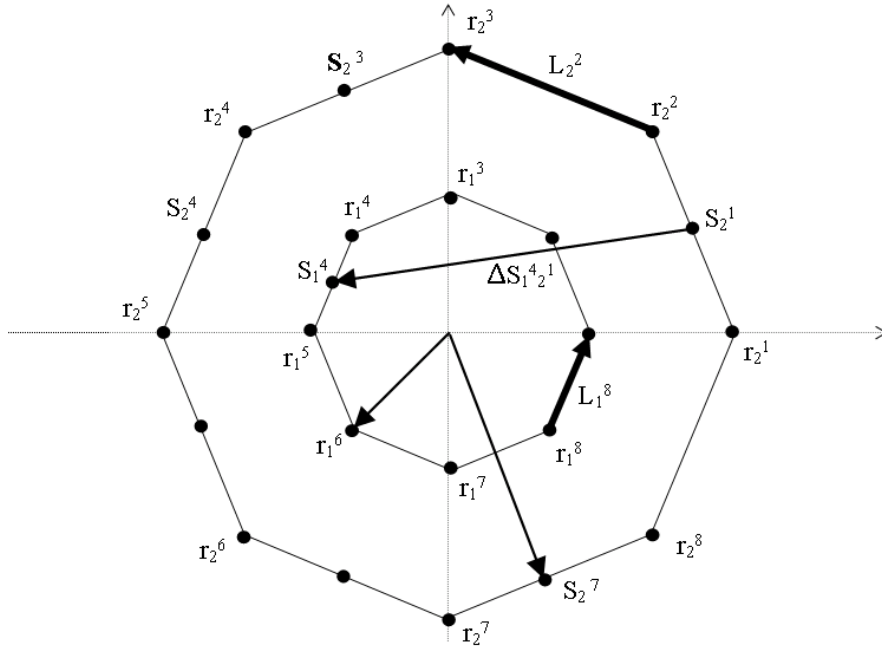


Fig. 5.— Definitions of variables on the segmented rings. Each ring is defined by N_i coordinates marked as r_i^m . Through these coordinates we define the segments: S_i^m , where each segment has a length vector L_i^m . The distance between segment S_i^m and segment S_j^n is defined as ΔS_{ij}^{mn} .